Powder Technology 294 (2016) 284–291

Contents lists available at ScienceDirect

Powder Technology

journal homepage: www.elsevier.com/locate/powtec

Coupling effect of chromia doping and vacuum on the phase transition of alumina prepared by co-precipitation process

Cheng Zeng [a], Yunhan Ling [a,*], Yakui Bai [a], Weifeng Liu [a], Yixiang Chen [b]

[a] Lab of Advanced Materials, School of Materials Sciences and Engineering, Tsinghua University, Beijing 100084, China
[b] Technical Institute of Physics and Chemistry, Chinese Academy of Sciences, Beijing 100190, China

ARTICLE INFO

Article history:
Received 25 August 2015
Received in revised form 22 January 2016
Accepted 26 February 2016
Available online 3 March 2016

Keywords:
Alumina
Chromia
Phase transition
Vacuum calcination

ABSTRACT

Synthesis of thermodynamically stable corundum structure alumina under lower temperature is of great significance in practical applications, exploration on new technique and the involved mechanism therefore becomes increasingly essential. In this work, the coupling effect and mechanism of chromia doping and vacuum condition on the phase transition of Al_2O_3 prepared via co-precipitation process were investigated and explored. It was found that chromia doping by itself did not promote the nucleation of α-Al_2O_3, or in some sense inhibited the transformation process. Cr doped γ-Al_2O_3 powders treated in a vacuum condition (10^{-5} Pa) however showed a gradual transition to α-Al_2O_3 even at low temperature of 600 °C, demonstrating that surface nucleation sites introduced by a coupled effect of vacuum and Cr_2O_3 doping contributed to the dramatic reduction (200–400 °C) of the phase transformation temperature. Based on the comprehensive characterizations and conventional diffusional nucleation mechanism, it is concluded that the surface nucleation sites for phase change to α-Al_2O_3 increased significantly during vacuum calcination with the combination of template effects of Cr_2O_3. This finding may provide a new way in fabrication and understanding of stable alumina formation under relatively moderate temperature condition.

1. Introduction

Due to many beneficial properties and several existing crystalline phases, alumina finds applications in a wide variety of areas, including heterogeneous catalysis, abrasives, ceramic materials and protective coatings [1,2]. For example, α phase is widely used as wear-resistant coatings due to its hardness and thermal stability, while γ phase is often used as catalysts or catalyst supports because of its low surface energy and high specific surface areas available for catalytic reactions [3,4]. Alumina exists in many different polymorphs–several transition phases (γ, κ, δ, θ, etc.) as well as the only thermodynamically stable phase α-Al_2O_3. Even though α-Al_2O_3 is thermodynamically stable at all temperatures up to its melting point, the transition phases are often formed at temperatures below 1000 °C. The reason seems to be that the transition phases are surface energy stabilized at lower temperatures [5]. Transformations between metastable phases are topotactic and therefore of relatively low energy [6]. The phase of θ-Al_2O_3, the most crystallographically ordered transition alumina, is often the final step before the transition to α-Al_2O_3 [7]. The transformation from θ-Al_2O_3 to α-Al_2O_3 involves a change in the oxygen sub-lattice from cubic to hexagonal close packing and generally ends in the transformation to the stable phase α-Al_2O_3above ~1100 °C. Generally, the transformation to α-Al_2O_3 obeys a classical nucleation and growth mechanism. A study by Messing et al. claims the evidence for a diffusional nucleation mechanism for the transformation of θ-Al_2O_3 to α-Al_2O_3 [7]. A critical crystal size, the most commonly reported evidence for a shear nucleation mechanism, is also necessary for the diffusional nucleation mechanism because the transition alumina must coarsen to produce potent heterogeneous alpha nucleation sites [8]. In addition, diffusional nucleation is more favorable at surfaces or other low energy sites and the energy barrier for diffusional nucleation arises from the creation of a new surface between the nucleating (α) and matrix (θ or γ) phases. The metastable phases are involved in the following common transition sequence as:

Bayerite or boehmite→γ-Al_2O_3→δ-Al_2O_3→θ-Al_2O_3→α-Al_2O_3.

The grains can grow fast at higher temperatures with these transformations and as a result there is a decrease of specific surface area and consequently loss of sinterability [9]. Moreover, an elevated temperature of higher than 1000 °C prohibits the use of α-Al_2O_3 coatings on temperature sensitive substrates such as many metals and their alloys [10]. Thus, there is a pressing demand for decreasing the growth temperature of α phase. Considerable studies have already been carried out on the phase transformation of alumina. It is well known that the phase transition of γ-Al_2O_3 to α-Al_2O_3 can be influenced by cation additive. For example, the gamma to alpha phase transition temperature

* Corresponding author.
E-mail address: yhling@mail.tsinghua.edu.cn (Y. Ling).

http://dx.doi.org/10.1016/j.powtec.2016.02.045
0032-5910/

was inhibited by the addition of monovalent cations — i.e., Li^+, Na^+ and K^+ [11], whereas the addition of transition metals such as Mn^{2+} and Cu^{2+} has been reported to accelerate the transformation, hence reducing the temperature [12]. Some other approaches have been proposed to prepare α-Al_2O_3 at lower temperatures and the corresponding mechanism has been investigated; by adding α-Fe_2O_3 or α-Al_2O_3 seed the energy for nucleation could be either reduced or overcome [13]. In this present work, Cr doped alumina powders were synthesized by a conventional co-precipitation process. Phase evolution of the precursors and the new coupling effect of chromia doping and vacuum calcination on the phase transformation of alumina and the involved mechanism were investigated.

2. Experimental procedure

2.1. Materials processing

In the present study, the starting materials for hydrated alumina are $Al(NO_3)_3 \cdot 9H_2O$ with a purity of 99% (by weight, wt.) and $Cr(NO_3)_3 \cdot 9H_2O$ with a purity of 99% (wt.). Aqueous ammonia solution (25 vol.%) of 99% (wt.) in purity was chosen as the precipitant. All these reagents were purchased from Sinopharm Chemical Reagent Co. Ltd., and used without further purification.

The flow chart of the preparation procedure is depicted in Fig. 1. $Al(NO_3)_3 \cdot 9H_2O$ and $Cr(NO_3)_3 \cdot 9H_2O$ were dissolved into deionized water. Precursors were prepared by dropping ammonia solution into the solution at a low speed under magnetic stirring at room temperature. When the slurry pH was adjusted to 9.0–10.0 by a pH test strip, it was stirred for another 30 min after finishing dropping. The resulting suspensions were aged for 12 h at room temperature, after which the slurry was rinsed with distilled water and ethyl alcohol two times respectively and then dried at 100 °C for 12 h. After an intermediate grinding, the dried gels were heat treated at 600 °C for 2 h in air to remove the hydroxyl species. The dehydrated samples show a pure phase of γ-Al_2O_3. Several samples of alumina containing 0, 1 wt.% and 3 wt.% chromium, corresponding to 0, 1.46, 4.38 mol% Cr_2O_3, were prepared in this manner, and the three samples with different doping concentrations will be denoted henceforth as 0%Cr, 1%Cr and 3%Cr. Fractional as-prepared powders were sealed in a high-vacuum quartz tube with a pressure of 5×10^{-5} Pa; the sealed and unsealed alumina powders were calcined at different temperatures for 4 h.

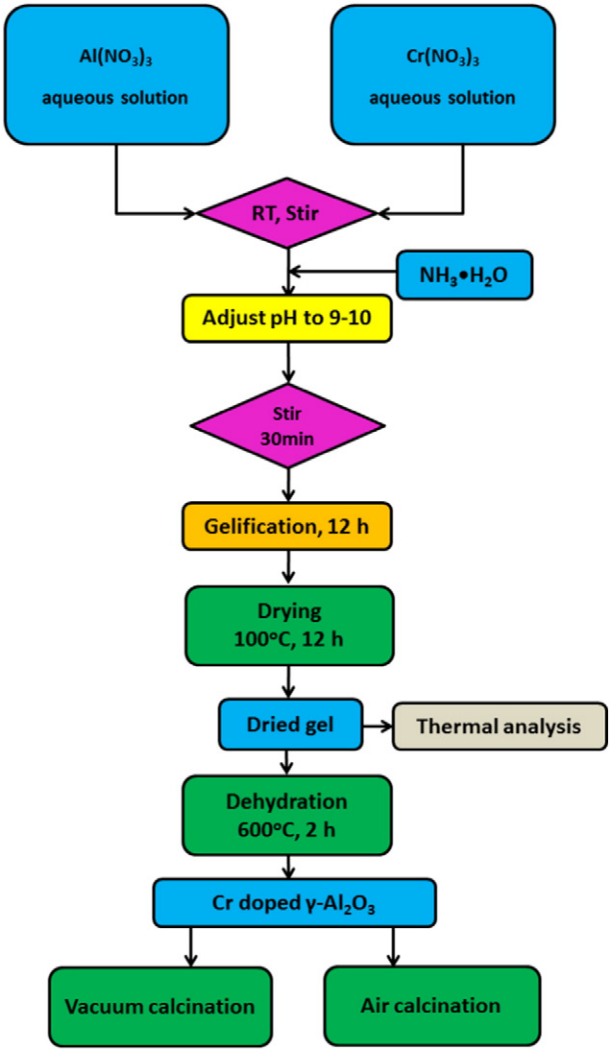

Fig. 1. Flow chart of the preparation procedure.

2.2. Powder characterization

Chemical compositions of these as-prepared γ-Al_2O_3 powders were verified by an X-ray Florescence spectrometer (XRF, XRF-1800, SHIMADZU, Japan). Differential scanning calorimetry (DSC) of the original precursors was employed to investigate the chromia doping effect.

Phase identification of the powders treated at different temperatures was performed on an X-ray diffractometer (D8 Advance, BRUKER, Germany) with Cu Kα radiation at a scanning speed of 6°- per minute. Photoluminescence (PL) measurements were carried out with a Raman spectrometer (Lab HR Evolution, HORIBA, France) using argon ion laser excitation at 532.2 nm and 632.8 nm at room temperature to detect the trace amount of α-Al_2O_3 and to analyze the Cr^{3+} luminescent states in both α-Al_2O_3 and γ-Al_2O_3, respectively [14,15]. Differential scanning calorimetry (DSC) was made on a DSC analyzer (STA449F3, NETZSCH, Germany) in flowing air with a heating rate of 10 °C/min and thermal gravimetric analysis (TG) used a TG analyzer (QMS403C, NETZSCH, Germany).

Several techniques were employed to explore mechanism of the coupling effect. Fourier transform infrared spectroscopy (FTIR) was measured on an infrared spectroscope (VERTEX 70V, BRUKER, Germany) with KBr pellet technique to study the different types of Al–O stretching and bending modes. Furthermore, the powders were ultrasonically treated for 20 min in alcohol. The pellucid solution was dripped onto an ultra-thin carbon coated copper grid for transmission electron microscopy (TEM, Tecnai G2 F30, FEI, US) characterization.

3. Results and discussion

3.1. Chromia doping effect

Fig. S1 shows the representative DSC and TG curves for the dried precursor of 0%Cr sample; the several peaks before 500 °C of the DSC profile are accompanied by a large weight loss on the TG curve. It is associated with loss of water. The TG curve indicates the complete decomposition of the precursors occurred near 700 °C. The wave near 500 °C of the DSC profile is due to the initial formation of γ-Al_2O_3; the three exothermic features 1, 2 and 3, observed at higher temperatures, correspond to the formation of other transition alumina. The broad peak centered at ~1000 °C may be related to the transition of γ-Al_2O_3 to δ-Al_2O_3, the well-defined peak at ~1100 °C corresponds to the transformation of δ-Al_2O_3 to θ-Al_2O_3 and the third thermal event at 1217 °C is the characteristic of the θ to α alumina transition [16]. For precursors of 0%Cr, 1%Cr and 3%Cr, similar curves were obtained over the range of 50–900 °C, and DSC curves are presented in Fig. 2 for different samples in the range of 900 °C–1300 °C. One can note that the last transformation was shifted to higher temperature for samples of 1%Cr (1260 °C) and 3%Cr (1272 °C). From the thermal analysis results, it suggests that

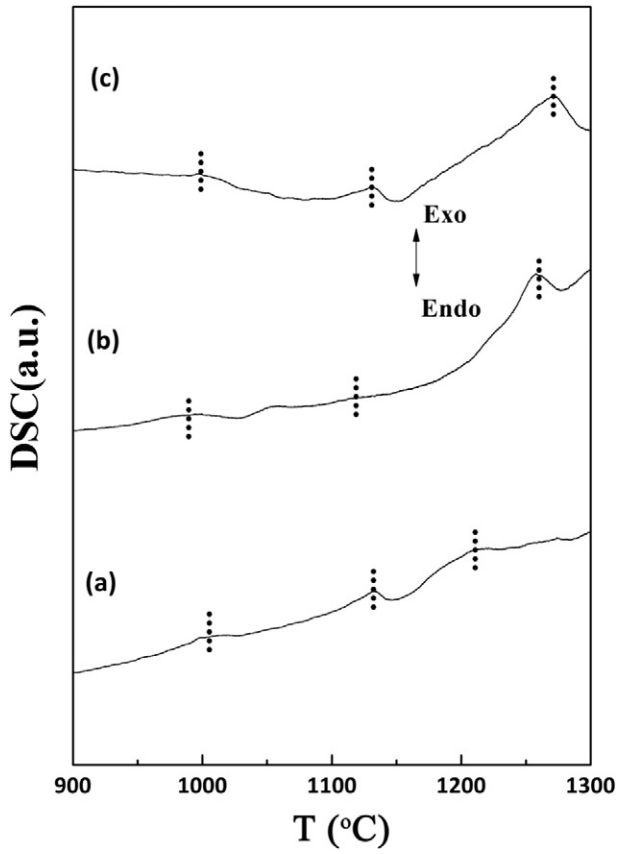

Fig. 2. Enlargement of the thermograms between 900 °C and 1300 °C for Cr doped alumina samples. (a) 0%Cr, (b) 1%Cr and (c) 3%Cr.

chromia doping may inhibit the final transformation to α-Al_2O_3. In addition, the XRD spectra of the 0%Cr, 1%Cr and 3%Cr heated at 1000 °C show that all the samples displayed the θ-Al_2O_3 structure. More specifically, lower-speed scanning of the strongest peak centered at ~67.4° was conducted to estimate the crystallite sizes for different chromia doping concentrations, and the results are depicted in Fig. S2. The estimated grain sizes determined from the refined XRD results are estimated by the Scherrer formula to be ~9 nm. It seems that although chromia doping by itself inhibits the phase transformation process of θ to α alumina, it does not affect the coarsening of theta alumina. Besides, compared with the peak position of samples 0%Cr and 1%Cr, there is a shift towards smaller angle (larger d-spacing) for sample 3%Cr calcined at 1000 °C, indicating a lattice expansion in the alumina lattice after chromia doping.

As for the chromia doping effect on the phase transformation to α-Al_2O_3, it is previously reported that dopant Cr^{3+} incorporated into the crystal structure could inhibit the transformation to α-Al_2O_3. The chromia doping effect was due to the resisting of the cooperative motion of the oxygen ions [7,17,18]. However, it has been extensively investigated that with external chromia acting as a template, the final transition to α-Al_2O_3 can occur at much lower temperatures, especially for α-Al_2O_3 films prepared through vapor deposition or magnetron sputtering deposition techniques [19–21]. It is generally accepted that both α-Al_2O_3 and chromia have the corundum-type structure (space group R3c). Chromia of the trigonal phase (Eskolaite: $a_0 = 0.5048$ nm, $c_0 = 1.3735$ nm [15]), which can be obtained at temperature about 600 °C, has lattice mismatches to α-Al_2O_3 ($a_0 = 0.4742$ nm, $c_0 = 1.2936$ nm [22]) of 6% and 5.8% for the a and c axes, respectively. Taking into account the almost equivalent cell parameters of chromia and α-Al_2O_3, it is reasonable to presume that the transformation to α-Al_2O_3 can be induced and promoted by the more easily formed chromia.

In short, chromia in the solid solution of $(Al, Cr)_2O_3$ acts as Cr^{3+} in a crystallographic environment under the distorted symmetry of ionic oxygen in transition Al_2O_3, rather than an independent corundum-type template. Given the larger ionic radius of Cr^{3+} (0.062 nm) over Al^{3+} (0.054 nm), the chromia doping causes a lattice expansion in the alumina lattice, as demonstrated in Fig. S2. Thus, it is inferred that the rearrangement of oxygen ions is suppressed and thus the cooperative motion of the ions, the rate controlling step of the transition to α-Al_2O_3, is restricted.

3.2. Vacuum calcination effect and coupling effect

Powders of 0%Cr and 1%Cr were used to study the vacuum calcination effect and coupling effect. The XRD patterns of powders calcined at 800 °C and 1000 °C for 4 h in vacuum and in air are summarized in Fig. 3. It can be seen that samples heated in vacuum transformed to α-Al_2O_3 at a much lower temperature. For instance, partial transformation to α-Al_2O_3 was observed for 0%Cr vacuum annealed at 1000 °C and 1%Cr vacuum annealed at 800 °C, and a complete transformation to α-Al_2O_3 was achieved for 1%Cr vacuum annealed at 1000 °C. It indicates that although chromia doping by itself inhibits the phase transition to α-Al_2O_3, chromia doping combined with vacuum calcination has a more favorable effect of accelerating the phase transformation to α-Al_2O_3 than the single vacuum calcination without chromia doping. The following discussion will be mainly focused on the coupling effect of vacuum calcination and chromia doping, i.e. the phase evolution of 1%Cr powders and the possible mechanism will be intensely discussed. To make it simple, the 1%Cr powders calcined at 800 °C in air and vacuum are henceforth denoted as S1 and S2, respectively.

To reiterate, all the as-prepared precursors were heated at 600 °C for 2 h to remove the hydroxyl species before further calcination and the XRD spectra confirm a pure γ-Al_2O_3 phase of the heated oxides. Fig. 4 depicts the TEM images and selected area electron diffraction (SAED) patterns of S1 and S2. Compared with the SAED patterns of S1, some other diffraction spots, assigned to α-Al_2O_3 planes of (214), (113) and θ-Al_2O_3 plane of (1 1 2), are indexed in the figure, indicating that θ-Al_2O_3 or α-Al_2O_3 may exist in S2. In addition, it is clear that the average crystallite size of the particles (10–20 nm) after vacuum calcination is much larger than that of particles (5–10 nm) after air calcination. Also, it should be mentioned that despite the absence of amorphous phase in XRD spectra, amorphous characteristic halos arise in the SAED patterns. The halos are probably attributed to the ultra-thin amorphous carbon supporting films used in the TEM analysis.

HRTEM images of S1 and S2 are given in Fig. 5. The d-spacing labeling results indicate that both S1 and S2 have the phase of θ-Al_2O_3. In addition, for S2 it appears that planes (113) and (024) of α-Al_2O_3 coordinate with the plane (112) of θ-Al_2O_3. However, only γ-Al_2O_3 and α-Al_2O_3 are sorted out in the XRD spectra. Thus, it suggests that there exists a tiny amount of the intermediate phase of θ-Al_2O_3 in S2, hence the transformation of θ-Al_2O_3 to α-Al_2O_3 swiftly completed for S2.

The XRD results (Fig. 3) indicate that the vacuum calcination combined with chromia doping can significantly reduce the transformation temperatures (at least 200 °C) of γ-Al_2O_3 to α-Al_2O_3. To locate the critical temperature related to the coupling effect, the vacuum calcination temperature of 1%Cr was lowered to 700 °C. The XRD result shows that a pure phase of γ-Al_2O_3 was obtained for 1%Cr after calcination in both vacuum and air at 700 °C. Generally, XRD analysis can identify the main phase, but it is impossible to screen out trace phases. Due to the significant luminescent ability of Cr^{3+} ions in α-Al_2O_3, it is assumed that the luminescence spectra could be an effective way to detect the trace amounts of α-Al_2O_3.

Fig. 6 presents the luminescence spectra of 1%Cr calcined at different temperatures. After vacuum calcination at 800 °C, a sharp and intense doublet, commonly labeled R_1 and R_2 at 692–695 nm was detected. The doublet phenomenon is attributed to the Cr^{3+} ions in a high

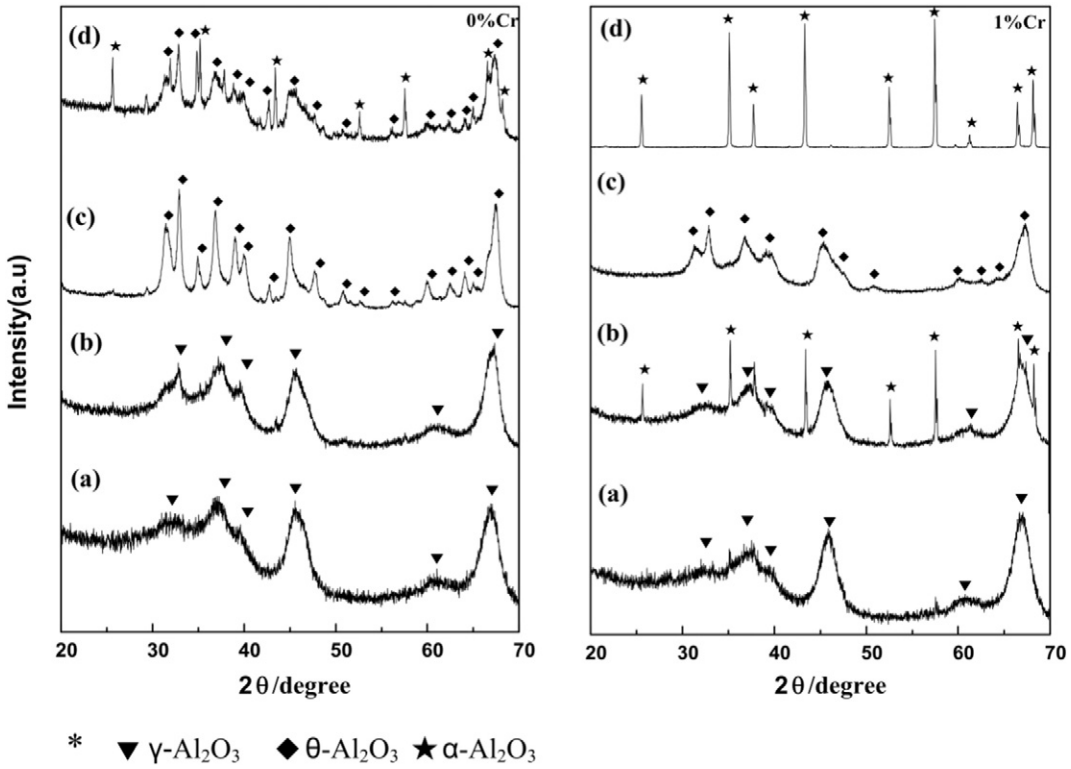

Fig. 3. XRD patterns of the 0%Cr and 1%Cr powders calcined for 4 h at (a) 800 °C, in air, (b) 800 °C, in vacuum, (c) 1000 °C, in air, and (d) 1000 °C, in vacuum.

crystal-field environment under the distorted octahedral symmetry of ionic oxygen in α-Al_2O_3 [23]. The doublet at the same wavelength position is also observed for 1%Cr after vacuum calcination at 700 °C and 600 °C, confirming that a phase transformation to α-Al_2O_3 occurs even at lower temperature of 600 °C. However, after vacuum calcination at 550 °C, the two distinct lines did not appear. Therefore, the critical temperature for the coupling effect should be positioned between 550 °C and 600 °C.

3.3. Mechanism discussion

Taking into account the results in subsections (3.1) and (3.2), it is demonstrated that compared to chromia doping effect, chromia doping coupled with vacuum calcination can better promote the phase transition to α-Al_2O_3. In order to investigate the inner mechanism, techniques regarding the characterization of electronic structures and Al–O bonds of the alumina powders were further employed.

Fig. 7 presents the PL spectra of 1%Cr calcined in different conditions using a 632.8-nm Ar excitation laser. It can be seen from Fig. 7(e) that the PL spectrum of 1%Cr after air calcination at 800 °C displayed a broad band (>700 nm) emission feature, which was attributed to the Cr^{3+} in a weak field situation of γ-Al_2O_3, as Lu and Kulinkin reported [24,25]. As for 1%Cr after vacuum calcination at 800 °C, the strongly inhomogeneously broadened spectra and a narrow doublet are observed simultaneously. The broad band remains unaltered after vacuum calcination, indicating that chromium ion states in γ-Al_2O_3 remain

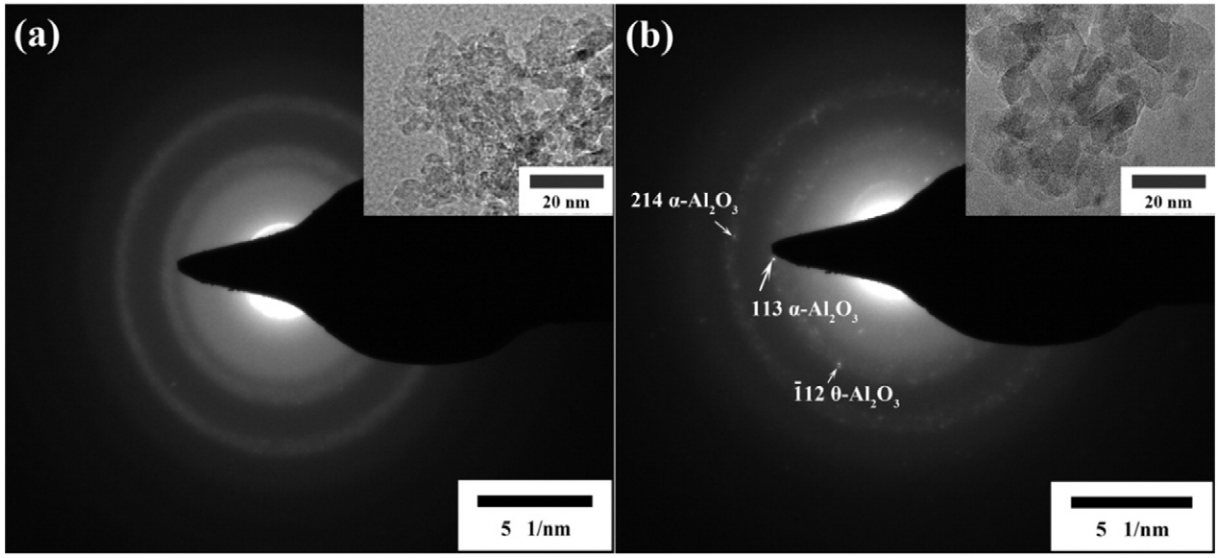

Fig. 4. Selected area electron diffraction and TEM photographs of the 1%Cr sample calcined at 800 °C for 4 h in (a) air and (b) vacuum.

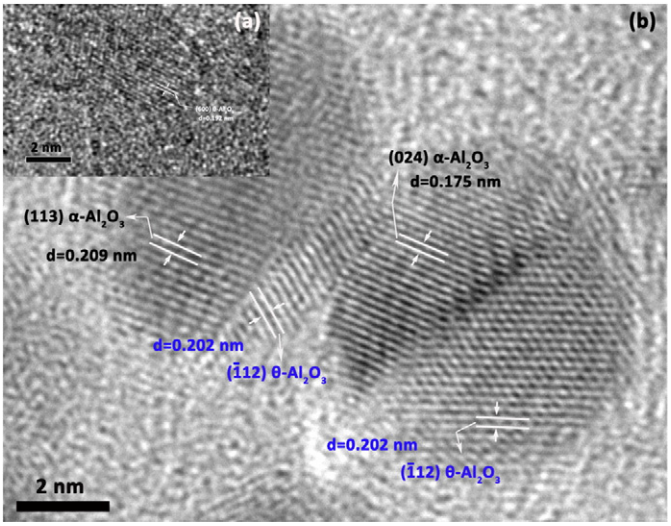

Fig. 5. High resolution image of (a) S1 and (b) S2.

almost unaffected. The sharp doublet corresponds to the R-lines ($^2E_g \rightarrow {}^4A_{2g}$) of Cr^{3+} in α-Al_2O_3, as observed in Fig. 6. Therefore, the 1%Cr powders after air calcination at 800 °C mainly comprise of Cr doped γ-Al_2O_3 whereas powders after vacuum calcination at 800 °C constitute Cr doped γ-Al_2O_3 and Cr doped α-Al_2O_3. The PL result is consistent with the XRD and TEM results as shown in Figs. 3 and 4. Additionally, features similar to that of 1%Cr vacuum calcined at 800 °C were observed for 1%Cr vacuum calcined at 700 °C and 600 °C, unfolding a predominant phase of γ-Al_2O_3 and α-Al_2O_3. When the

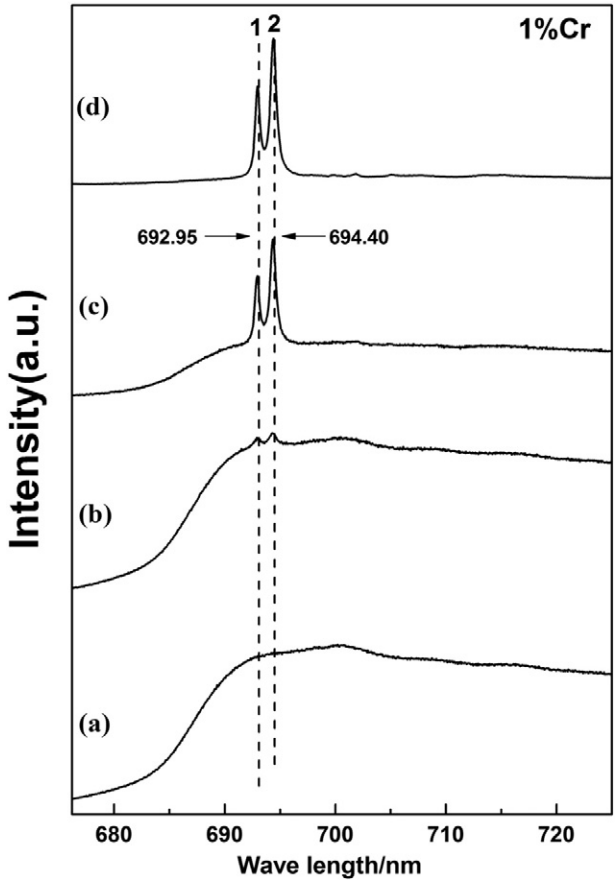

Fig. 6. Luminescence spectra of the 1%Cr sample calcined in vacuum for 4 h at (a) 550 °C, (b) 600 °C, (c) 700 °C, and (d) 800 °C.

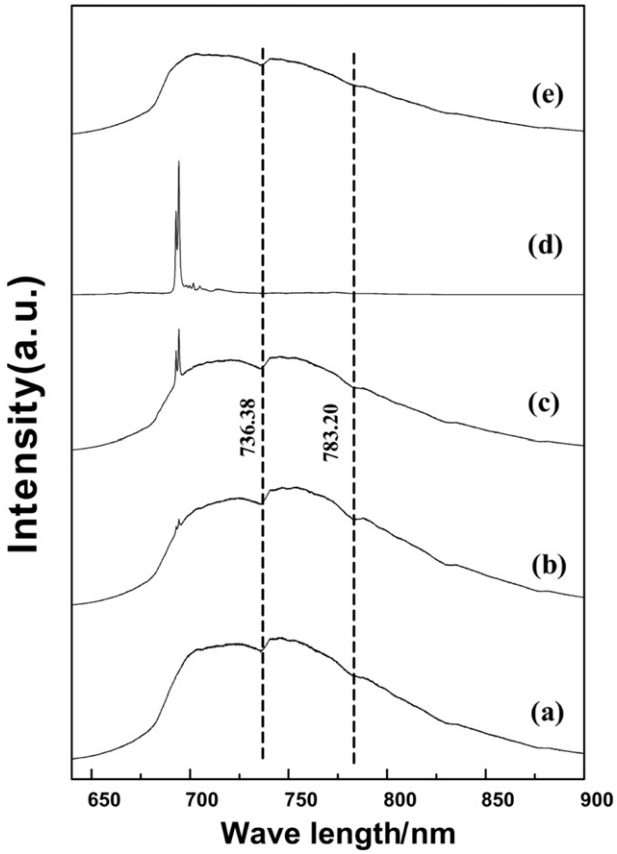

Fig. 7. PL spectra of the 1%Cr sample calcined for 4 h at (a) 600 °C, in vacuum, (b) 700 °C, in vacuum, (c) 800 °C, in vacuum, (d) 1200 °C, in air, and (e) 800 °C, in air.

1%Cr powders were sintered in air at 1200 °C, a characteristic curve attributed to a pure phase of chromia doped α-Al_2O_3 emerged. However, in comparison with the powders sintered in air at 1200 °C (R_1 at 692.91 nm, R_2 at 694.32 nm), there is a red shift of R-line frequency for the powders after vacuum calcination (R_1 at 692.92 nm, R_2 at 694.37 nm). Scientifically, the increase in the R-line frequency is ascribed to the stronger crystal field at Cr^{3+} ions in α-Al_2O_3, which is commonly interpreted by a lattice expansion of the alumina due to chromia doping [23,26]. In our study of the coupling effect, the chromia doping concentration is fixed to 1 wt.% chromium (1.46 mol% chromia). Therefore, the red shift of R-lines after vacuum calcination aroused by a weaker crystal field at Cr^{3+} ions probably resulted from the formation of weaker Cr–O bonds in α-Al_2O_3.

In order to give an insight into the mechanism, FTIR analysis concerning the Al–O bonding strength in the bulk was implemented. Fig. 8 presents the FTIR spectra of S1, S2 and two other reference samples, i.e. 1%Cr sintered at 1000 °C with the main phase of θ-Al_2O_3 (denoted as S3) and 1%Cr sintered at 1200 °C with the phase of α-Al_2O_3 (denoted as S4), respectively. It is previously reported that in aluminum oxides, if the coordination is octahedral (AlO_6), the Al–O stretching and bending modes are expected in 500–750 cm^{-1} and 330–450 cm^{-1}, respectively. Nevertheless, a tetrahedral coordination (AlO_4) is expected to give stretching modes between 750 and 850 cm^{-1} and bending modes in the narrow range 250–320 cm^{-1} [27].

In the infrared spectrum of S4, peaks at 721, 638 and 588 cm^{-1} are assigned to the stretching modes of AlO_6, while the bands observed at 492 and 447 cm^{-1} are assigned to the bending modes of AlO_6. It is evident that S4 simply contains octahedral Al–O coordination, indicating a pure phase of chromia doped α-Al_2O_3 [28]. Comparing the infrared spectra of S1 and S3, they both include three peaks at 829, 768 and 567 cm^{-1}, but with different fine structures. Compared to S3, the peaks of S1 are much broader, probably because of the surface

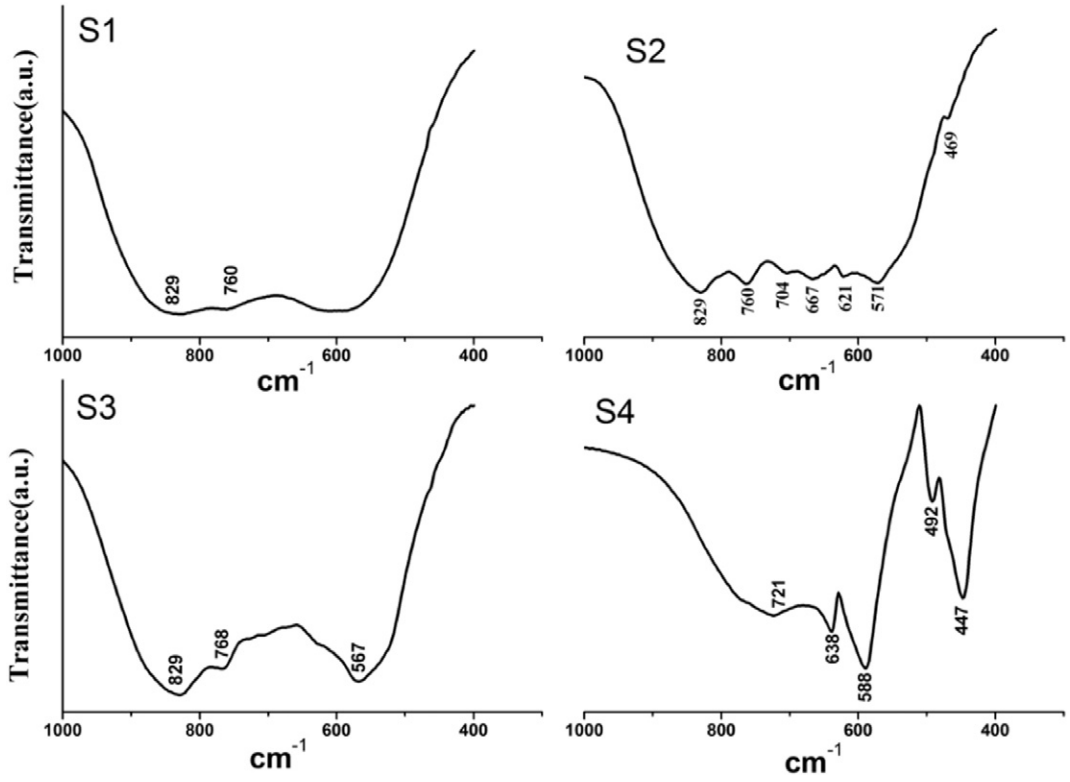

Fig. 8. FTIR spectra for S1, S2, S3 and S4.

effect or the increasing dangling bonds caused by a smaller grain size [27,29]. As for S2, given its phase compositions of γ-Al_2O_3, θ-Al_2O_3 and α-Al_2O_3, the peaks are assigned into three different groups. According to the spectra of S1, S3 and S4, it is safe to infer that peaks at 829 and 760 cm^{-1} were attributed to the AlO_4 stretching modes of θ-Al_2O_3 or γ-Al_2O_3, and the band at 469 cm^{-1} belongs to the AlO_6 bending modes in γ-Al_2O_3, as documented in the literature [27]. Also, compared with the spectra of S2, it is obvious that peaks assigned to γ-Al_2O_3 for S1 are much broader, indicating a much smaller grain size of S1 [29]. In terms of the stretching modes of AlO_6 for S2, the band observed at 667 cm^{-1} is probably attributed to the AlO_6 stretching modes in θ-Al_2O_3, whereas the bands at 704, 621 and 571 cm^{-1} are attributed to the AlO_6 stretching modes in α-Al_2O_3. Additionally, in comparison of the spectra of S4 and S2, it can be seen that there is a 17 cm^{-1} frequency shift of the AlO_6 stretching modes in α-Al_2O_3, i.e. from 721, 638 and 588 cm^{-1} in S4 to 704, 621 and 571 cm^{-1} in S2, respectively. Consequently, the vacuum calcination leads to a weaker Al–O bonding in α-Al_2O_3, in good accordance with the PL spectra. The vibrational frequencies are summarized in Table 1.

Table 1
Observed vibrational transitions (cm^{-1}) and assignments for S1–S4.

S1	S2	S3	S4	Assignments
829	829	829		ν AlO_4
760	760	768		
	704		721	ν AlO_6
	667			
	621		638	
	571	567	588	
	469		492	δ AlO_6
			447	

ν, stretching; δ, bending.

To give a possible mechanism of the coupling effect, some important postulates and results are listed, as follows:

- Chromium is uniformly incorporated into the alumina prepared via a conventional co-precipitation process, and no obvious migration during calcination.
- Phase transformation to α-Al_2O_3 in our experiment obeys the diffusional nucleation mechanism. A critical crystal size is necessary and diffusional nucleation is more favorable at surfaces or other low energy sites.
- The average crystallite size of γ-Al_2O_3 after vacuum calcination is larger than that of air calcination, as determined by TEM and FTIR results.
- For S2, the phase transformation of θ-Al_2O_3 to α-Al_2O_3 is quickly completed, as demonstrated by the HRTEM and XRD results.
- Compared to S1, weaker Al–O and Cr–O bonds in α-Al_2O_3 were obtained in S2, as confirmed by PL and FTIR results.

Heating in a rarefied environment will be conducive to molecular or ionic desorption from solid surface. Liu et al. reported F^+ center emission (an oxygen-ion vacancy occupied by two electrons) in γ-Al_2O_3 derived by thermal dehydration of boehmite, similar to the case in our study [30]. Therefore, the vacuum calcination effect is probably due to the increase of oxygen vacancy concentration, which may introduce new surface nucleation sites. Thus, the increase of nucleation density followed by an increase of the diffusional growth rate reduces the incubation time to form a 'critical size'.

As discussed in subsection (3.1), the inhibition of transformation to α-Al_2O_3 caused by chromia doping is probably ascribed to the larger size of chromium ions over aluminum ions, i.e. chromium ions are restricted in the alumina lattice and thereby cannot act as a template like the independent hexagonal phase of chromia. Based on the comprehensive results, a possible mechanism is proposed to interpret the coupling effect according to the observed results and the classic phase transformation theory.

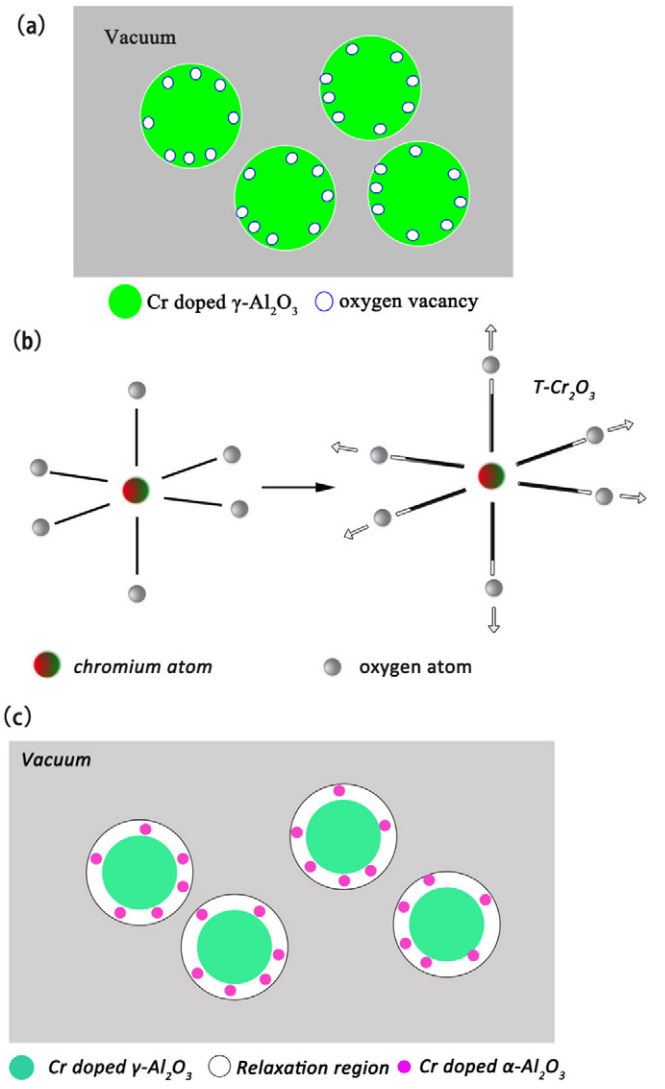

Fig. 9. Schematic illustration of the possible mechanism of phase change from γ-Al_2O_3 to α-Al_2O_3 based on the coupling effect.

Fig. 9 (a)–(c) presents schematics of the sequence of the transformation to α-Al_2O_3 on the basis of coupling effect. Fig. 9 (a) shows the initial configuration of the Cr doped γ-Al_2O_3 powders. It is probably due to the increasing oxygen vacancies on the surface of γ-Al_2O_3 grains during vacuum calcination that more favorable surface nucleation sites are generated. In the next stage, together with the increase of new nucleation sites, it is inferred that surface relaxation occurs on the surface of γ-Al_2O_3 grains, causing an extension of the Cr–O and Al–O bonding. As a result, the restrained Cr–O bonds transform to a state approximate to the CrO_6 state (octahedral Cr–O coordination) in the hexagonal phase Cr_2O_3, which can be regarded as a template for α-Al_2O_3 nucleation. The transitional state of CrO_6 during vacuum calcination is denoted as T-Cr_2O_3, as shown in Fig. 9 (b). Aside from the rising nucleation sites introduced by vacuum calcination, the nucleation barrier for the formation of α-Al_2O_3 nuclei is also reduced by the occurrence of T-Cr_2O_3 and the transformation to α-Al_2O_3 is readily completed, as shown in Fig. 9(c). Briefly, the coupling effect can dramatically enhance the kinetic rate of the phase transformation from γ-Al_2O_3 to α-Al_2O_3, leading to a distinct temperature reduction (at least 200 °C) in the inauguration of phase evolution. We believe that this finding will provide a promising technique and some new insights in the fabrication of thermodynamically stable alumina in forms of either powders or coatings under relatively moderate temperature condition.

4. Conclusions

In summary, nanoscale Cr doped Al_2O_3 powders were successfully prepared by using $Al(NO_3)_3$ and $Cr(NO_3)_3$ as the precursors via co-precipitation process and the coupling effect of the chromia doping and vacuum calcination on the phase transition of Al_2O_3 was scrutinously investigated. It may be safe to draw the following conclusions:

(1) Chromia doping by itself inhibits the phase transformation to α-Al_2O_3, probably due to the resistance of cooperative motions of the ions caused by the larger ionic radius of chromium ions over aluminum ions.
(2) Vacuum calcination can accelerate the phase transformation to α-Al_2O_3, and the chromia doping coupled with the vacuum calcination significantly reduces the phase transition temperature by 200–400 °C.
(3) A novel possible mechanism based on the surface reconstruction and classic phase transformation theory is proposed to interpret the coupling effect.

Acknowledgment

This research was funded by the State Key Laboratory of Surface and Chemistry, China Academy of Engineering Physics (No. SPC 201102), the National Basic Research Program of China (973 Program) under grant No. 2011CB61050, the NSAF program (No. U1430118), the Chinese National Fusion Project for ITER (No. 2013GB110000) and the 56th China Postdoctoral Science Foundation (Grant No. 2014M560980).

Appendix A. Supplementary data

Supplementary data to this article can be found online at http://dx.doi.org/10.1016/j.powtec.2016.02.045.

References

[1] B.L. Moroz, P.A. Pyrjaev, V.I. Zaikovskii, V.I. Bukhtiyarov, Nanodispersed Au/Al_2O_3 catalysts for low-temperature CO oxidation: results of research activity at the Boreskov Institute of Catalysis, Catal. Today 144 (2009) 292–305.
[2] S.B. Gurel, A. Altun, Reactive alumina production for the refractory industry, Powder Technol. 196 (2009) 115–121.
[3] A.R. Keshavarz, M. Rezaei, F. Yaripour, Nanocrystalline gamma-alumina: a highly active catalyst for dimethyl ether synthesis, Powder Technol. 199 (2010) 176–179.
[4] C.F. Chen, Z.D. Ding, Q. Tan, H.H. Qi, Y.H. He, Preparation of nano alpha-alumina powder and wear resistance of nanoparticles reinforced composite coating, Powder Technol. 257 (2014) 83–87.
[5] J.M. McHale, A. Auroux, A.J. Perrotta, A. Navrotsky, Surface energies and thermodynamic phase stability in nanocrystalline aluminas, Science 277 (1997) 788–791.
[6] I. Levin, D. Brandon, Metastable alumina polymorphs: crystal structures and transition sequences, J. Am. Ceram. Soc. 81 (1998) 1995–2012.
[7] R.B. Bagwell, G.L. Messing, P.R. Howell, The formation of alpha-Al_2O_3 from theta-Al_2O_3: the relevance of a "critical size" and: diffusional nucleation or "synchro-shear"? J. Mater. Sci. 36 (2001) 1833–1841.
[8] T.D. Isfahani, J. Javadpour, A. Khavandi, R. Dinnebier, M. Goodarzi, H.R. Rezaie, Mechanochemical synthesis of alumina nanoparticles: formation mechanism and phase transformation, Powder Technol. 229 (2012) 17–23.
[9] R.K. Pati, J.C. Ray, P. Pramanik, A novel chemical route for the synthesis of nanocrystalline alpha-Al_2O_3 powder, Mater. Lett. 44 (2000) 299–303.
[10] D.L. Smith, J. Konys, T. Muroga, V. Evitkhin, Development of coatings for fusion power applications, J. Nucl. Mater. 307 (2002) 1314–1322.
[11] K. Okada, A. Hattori, Y. Kameshima, A. Yasumori, R.N. Das, Effect of monovalent cation additives on the gamma-Al_2O_3-to-alpha-Al_2O_3 phase transition, J. Am. Ceram. Soc. 83 (2000) 1233–1236.
[12] K. Okada, A. Hattori, T. Taniguchi, A. Nukui, R.N. Das, Effect of divalent cation additives on the gamma-Al_2O_3-to-alpha-Al_2O_3 phase transition, J. Am. Ceram. Soc. 83 (2000) 928–932.
[13] J.L. McArdle, G.L. Messing, Transformation, microstructure development, and densification in alpha-Fe_2O_3-seeded boehmite-derived alumina, J. Am. Ceram. Soc. 76 (1993) 214–222.
[14] T. Li, S.G. Yang, Y.W. Du, Strongly luminescent Cr-doped alumina nanofibres, Nanotechnology 16 (2005) 365–368.
[15] M. Catti, G. Sandrone, G. Valerio, R. Dovesi, Electronic, magnetic and crystal structure of Cr_2O_3 by theoretical methods, J. Phys. Chem. Solids 57 (1996) 1735–1741.

[16] J. Li, Y.B. Pan, C.S. Xiang, Q.M. Ge, J.K. Guo, Low temperature synthesis of ultrafine alpha-Al_2O_3 powder by a simple aqueous sol–gel process, Ceram. Int. 32 (2006) 587–591.
[17] G.C. Bye, G.T. Simpkin, Influence of Cr and Fe on formation of alpha-Al_2O_3 from gamma-Al_2O_3, J. Am. Ceram. Soc. 57 (1974) 367–371.
[18] J.M. Andersson, E. Wallin, V. Chirita, E.P. Munger, U. Helmersson, Ab initio calculations on the effects of additives on alumina phase stability, Phys. Rev. B 71 (2005).
[19] E. Wallin, T.I. Selinder, M. Elfwing, U. Helmersson, Synthesis of alpha-Al(2)O(3) thin films using reactive high-power impulse magnetron sputtering, EPL 82 (2008).
[20] P. Jin, G. Xu, M. Tazawa, K. Yoshimura, D. Music, J. Alami, U. Helmersson, Low temperature deposition of alpha-Al_2O_3 thin films by sputtering using a Cr_2O_3 template, J. Vac. Sci. Technol. A 20 (2002) 2134–2136.
[21] J. Cai, B. Xu, G. Ling, Observation on the Interface of alpha-Al_2O_3/Cr_2O_3: prepared by oxidation of $Al_{45}Cr_7$, Appl. Surf. Sci. 268 (2013) 111–116.
[22] M. Catti, G. Valerio, R. Dovesi, M. Causa, Quantum-mechanical calculation of the solid-state equilibrium MgO + alpha-Al_2O_3-reversible-arrow-$MgAl_2O_4$ (spinel) versus pressure, Phys. Rev. B 49 (1994) 14179–14187.
[23] B. Henderson, G. Imbusch, Optical Spectroscopy of Inorganic Solids, Clarendon Press, Oxford, 1989.
[24] L. Shen, C. Hu, S. Zhou, A. Mukherjee, Q. Huang, Phase-dependent photoluminescence behavior of Cr-doped alumina phosphors, Opt. Mater. 35 (2013) 1268–1272.
[25] A.B. Kulinkin, S.P. Feofilov, R.I. Zakharchenya, Luminescence of impurity 3d and 4f metal ions in different crystalline forms of Al_2O_3, Phys. Solid State 42 (2000) 857–860.
[26] H.J. Yu, D.R. Clarke, Effect of codoping on the R-line luminescence of Cr^{3+}-doped alumina, J. Am. Ceram. Soc. 85 (2002) 1966–1970.
[27] C.H. Shek, J.K.L. Lai, T.S. Gu, G.M. Lin, Transformation evolution and infrared absorption spectra of amorphous and crystalline nano-Al_2O_3 powders, Nanostruct. Mater. 8 (1997) 605–610.
[28] G.K. Priya, P. Padmaja, K.G.K. Warrier, A.D. Damodaran, G. Aruldhas, Dehydroxylation and high temperature phase formation in sol–gel boehmite characterized by Fourier transform infrared spectroscopy, J. Mater. Sci. Lett. 16 (1997) 1584–1587.
[29] C.S. Zhang, F. Zhao, J.J. Zhang, X.Y. Wang, G.L. Bao, Infrared spectroscopic studies of alumina on a nanometer scale, Acta Chim. Sin. 57 (1999) 275–280.
[30] S. Liu, L. Zhang, Y. Fan, J. Luo, P. Zhang, L. An, Ultraviolet irradiation-induced photoluminescence degradation in gamma-alumina nanoparticles, Appl. Phys. Lett. 89 (2006).